Effects of high pressure treatments (ultra-high hydrostatic pressure and high pressure homogenization) on bighead carp (Aristichthys nobilis) myofibrillar protein native state and its hydrolysate

Mengting Chen
Huazhong Agricultural University
Lan Wang
Hubei Academy of Agricultural Sciences
Changliang Zheng
Hubei Academy of Agricultural Sciences
Wenjin Wu (wuwenjin@hbaas.com)
Hubei Academy of Agricultural Sciences

Research Article

Keywords: Ultra-high hydrostatic pressure, High pressure homogenization, Myofibrillar structure modification, Enzymatic hydrolysate, Antioxidant activity

Posted Date: May 26th, 2022

DOI: https://doi.org/10.21203/rs.3.rs-1672016/v1

Abstract

The impacts of four treatments ultra-high hydrostatic pressure (UHP), high pressure homogenization (HPH), combined UHP + HPH (U-H), and HPH + UHP (H-U) on bighead carp (*Aristichthys nobilis*) myofibrillar protein (BMP) structure, functional hydrolysis property to pepsin, and antioxidant activity of hydrolysates were investigated. All treatments led to increase in low-molecular-weight BMP, the BMP stability, and hydrophobic group exposure, but decrease in total sulfhydryl content and BMP particle size, thus resulting in increased hydrolysis and antioxidant capacity of enzymatic hydrolysates. U-H treated BMP exhibited the highest surface hydrophobicity (924.5 ± 1.0), zeta potential absolute value (18.88 ± 0.11 mV), hydrolysis degree (54.5 ± 1.6%), and antioxidant activity, but the lowest α-helix (21.84 ± 2.61%), intrinsic fluorescence spectrum intensity, total sulfhydryl (7.24 ± 0.07 μmol/g), and mean particle size (182.57 ± 2.23 nm). Therefore, U-H might be a promising pretreatment to prepare bioactive peptide.

1 Introduction

China is a major aquatic product country in the world with abundant freshwater fish resources. In 2020, the total production of freshwater fish farming reached 30.88 million tons. Bighead carp *(Aristichthys nobilis)* is one of the four major freshwater fish, and its total aquaculture output in 2020 accounted for 11.13% of the total freshwater fish aquaculture output in China. Bighead carp is rich in protein, lipids, and minerals. Its protein is an ideal source of essential amino acids for the human body, and its lipids are a desirable source of unsaturated fatty acids, thus it is of great economic value (Dai et al. 2021). Guo et al. (2008) reported that bighead carp not only plays a vital role in functional foods, but also has a protective effect on the human cardiovascular system. The head of bighead carp is the most commonly consumed part, and its tail is generally used as a by-product to make surimi or feed, whose value is not fully utilized.

The transformation from aquatic proteins to bioactive peptides through chemical extraction, fermentation, synthesis, and enzymatic hydrolysis is an effective by-product utilization approach (Ryan et al. 2011). Enzymatic hydrolysis is one of the most commonly used methods to prepare active substances (Wen et al. 2020), while its industrial application is limited due to its long time consumption and low hydrolysis rate. Appropriate treatments could change the protein structure to improve enzymatic hydrolysis efficiency. The methods to modify protein structure mainly include physical, chemical, enzymatic methods as well as biological engineering method (Tsumura et al. 2005). The physical treatment is convenient, simple, and environment-friendly, and thus it is more suitable for food industry (Liu et al. 2021). Ultra-high hydrostatic pressure (UHP) and high-pressure homogenization (HPH) are two common non-thermal physical modification methods. Non-thermal physical modification is a processing method in which physical forces such as shear, high pressure, ultrasound are applied to food and do not expose it to the adverse effects of heat, including high hydrostatic pressure, pulsed electric field, high intensity ultrasound, etc. (Sunil et al. 2018).

As an processing technology, UHP can make the protein structure looser, more cleavage sites exposed by changing non-covalent bonds such as hydrogen bonds and ionic bonds (Ulug et al. 2021). Meanwhile,

UHP is susceptible to induce protein aggregation via disulfide bonds (Gaoshang et al. 2019). Therefore, the susceptibility of protein to enzyme was changed. HPH treatment is a dynamic high pressure processing technology, and it is widely applied in microbial inactivation, submicron emulsion processing, and protein engineering (Saricaoglu et al. 2018). Under HPH treatment, the tertiary structure of protein will be changed (Liu et al. 2021), and the particle size of protein molecules is significantly reduced to the micron/submicron range due to the mechanical forces (shear, cavitation, turbulence, surface static electricity) (Chen et al. 2016), thus leading to more hydrophobic groups and cleavage sites are exposed to protease (Zou et al. 2020). In summary, the previous studies mainly focus on the effect of individual physical treatment on the functional properties of protein, whereas combined treatments will probably make full use of the advantages of individual techniques to improve the hydrolysis efficiency and final quality of enzymatic hydrolysates.

Myofibrillar protein accounts for 60% of the total protein in muscle tissue, and contributing to about 70% the nutritional value of fish meat (Xing et al. 2019). It would have been important to have more details about the structure of the proteins in the coproducts of these study and to have more specific reference about the use of static and dynamic pressure applied to myofibrillar protein (modification of structure) and proteolysis. The objectives of this study were to investigate the effects of four treatments ultra-high hydrostatic pressure treatment (UHP), high-pressure homogenization treatment (HPH), UHP followed by HPH (U-H), and HPH followed by UHP (H-U) on the microstructure and physicochemical properties of myofibrillar protein as were antioxidant activity of enzymatic hydrolysates in bighead carp *(Aristichthys nobilis)*.

2 Materials And Methods

2.1 Materials

Fresh live bighead carp were purchased from the local market (Wuhan, Hubei, China) and transported alive to the laboratory in oxygenated bags with water within 20 min. The fish were treated in ice water to death, then scaled, eviscerated, decapitated, chopped, and frozen to -80℃ for subsequent experiments. The entire experimental procedure followed the research protocols approved by the Institutional Animal Care and Use Committee of Huazhong Agricultural University (Wuhan, Hubei, China). Pepsin with an enzyme activity of 10,000 U/g was purchased from Guangzhou Saiguo biotech Co., LTD (Guangzhou, China). Sample buffer and molecular weight markers were bought from Tiangen (Beijing, China). All the chemicals and reagents such as the anilino-8-naphthalenesulfonate (ANS), tris hydrochloride, and maleic acid were of analytical and HPLC grades.

2.2 Preparation of bighead carp myofibrillar proteins (BMP)

Extraction of BMP was performed on ice by previously reported method with some modifications (Li et al. 2021b). Briefly, the samples were stored at -80℃, and thawed in a refrigerator at 4℃ for 18 h prior to extraction. The minced meat from bighead was washed with 0.02 M Tris-Maleate (pH 7.0) at the rate of

1:10 (w/v) and 6,000 r/min in a waring blender for 60 s. After filtration with 300 mesh gauze, the precipitate was rewashed with 0.02 M Tris-Maleate under the same blending and filtration conditions as described above. The precipitate was resuspended in 0.6 M Tris-Maleate (pH 7.0) for 18 h at 4℃ with interval stirring. The mixture was centrifuged at 12,000 g at 4℃ for 20 min. The supernatant was washed with 10 vol (w/v) ultrapure water and centrifuged at 12,000 g for 20 min. The precipitate was washed twice more under that same condition. The precipitate from the last centrifugation was bighead carp myofibrillar protein (BMP), which was stored at 4℃ before use. The Bradford method was used to measure the protein concentration, and the protein concentration of the precipitates was 12.0 mg/mL approximately.

2.3 BMP treatment

2.3.1 Ultra-high hydrostatic pressure (UHP) treatment

The BMP samples were placed in a pressure container filled with water and then treated at 300 MPa for 20 min. Pressure container temperature was maintained at 4℃. One portion of the treated samples were stored at 4℃ and the other portion was lyophilized and stored at -20℃ for subsequent use. Non-UHP treatment BMP was used as control (0.1 MPa). These pressurization parameters were chosen from the results of pre-experiments.

2.3.2 High pressure homogenization (HPH) treatment

The BMP was homogenized twice at 30 MPa in a continuous laboratory-scale high pressure homogenizer (ATS AH-2010, Suzhou, China). Following each homogenization, the BMP dispersion liquid was rapidly cooled to 4 ± 2°C in an ice-water bath. The untreated BMP was used as a control (0.1 MPa). Finally, the samples were stored or lyophilized for further analysis.

2.3.3 UHP followed by HPH (U-H treatment)

Following the same treatment operations in 2.3.1. and 2.3.2, the BMP dispersion liquid post UHP was then subjected to HPH.

2.3.4 HPH followed by UHP (H-U treatment)

H-U treatment conditions were the same with U-H ones with a reverse sequence of HPH and UHP.

2.4 Enzymatic hydrolysis

Following the above-mentioned treatment, pepsin (4000 u/g) was added to the BMP solution (pH 3.0), and reaction was performed at 55℃ for 6 h. The hydrolysis reaction was stopped in a water bath at 95℃ within 10 min. The hydrolysate was centrifuged at 10,000 g for 20 min, and the supernatant was collected. These enzymatic hydrolysis conditions were determined by the results of pre-experiments.

2.5 Total sulfhydryl content (SH_T)

The total sulfhydryl content was determined in reference to the method reported in previous study (Liu et al. 2000) with slight modifications. The 1.0 mL protein sample solution was mixed with 9.0 mL Tris-HCl buffer (0.2 mol/L, pH 7.0) containing 8 mol/L urea, 10 mmol/L EDTA, 2% SDS. After 30-min standing, the 4.0 mL mixture solution was further mixed with 0.4 mL DTNB (0.1%, pH 8.0). After 25-min reaction at 40℃, the absorbance of the mixture was measured at 412 nm. The molar extinction coefficient of 13600 L• (mol • cm)$^{-1}$ was used to calculate the SH_T.

2.6 Fourier Transform infrared spectroscopy (FT-IR)

The attenuated total reflection spectra of the lyophilized sample of BMP were obtained within the wavenumber range of 600 to 4000 cm^{-1} (Nicolet Is50 Fourier transform infrared spectroscopy, Germany) in reference to the previous study with minor modifications (Sharifian et al. 2019). The spectra were fitted within 1700-1600 cm^{-1} using Peakfit Version 4.04 to obtain gaussian curve (SPSS Inc., Chicago, Il, USA). Prior to curve fitting, the data were subtracted from the linear baseline, and Fourier deconvolution was used to differentiate the peak locations. The secondary structures (α-helix, β-sheet, β-turn, and random coil) were calculated according to the curve fitting results.

2.7 Intrinsic Fluorescence Emission Spectroscopy (IFES)

The intrinsic fluorescence is used to evaluate the "denaturation state" of proteins by targeting aromatic amino acids, mainly tryptophan. Fluor photometer (F-7000, Hitachi, Japan) was used to monitor BMP dispersion (0.3 mg/mL) by the previously reported method with minor modifications (Shi et al. 2019). The excitation wavelength was 280 nm and the monitoring range of emission spectrum was from 270 to 450 nm. The scan speed and slit width were 2400 nm/min and 2.5 nm, respectively.

2.8 Surface Hydrophobicity (H_0)

ANS titration method was used to measure the surface hydrophobicity (H_0) of BMP solution (Haskard and Li-Chan 1998). Different treated BMPs were diluted to the concentrations ranging from 0.1 mg/mL to 0.5 mg/mL with 0.6 M Tris-maleate buffer (pH 7.0). The 2.0 mL of BMP solution was mixed with 10.0 μL of ANS solution (8.0 mmol/L in 0.1 mol/L sodium phosphate buffer, pH 7.0) and reacted for 30 min. A fluorescence spectrophotometer (F-7000, Hitachi, Japan) was used to determine the relative fluorescence intensity at 385 nm excitation wavelength and at 470 nm emission wavelength (slit 3 nm). The initial slope of the fluorescence intensity versus protein concentration curve (calculated by linear regression analysis) was defined as the value of H_0.

2.9 Particle size distribution and zeta potential

The particle size and zeta potential of BMP were determined using photon correlation spectroscopy (Zetasizer Nano ZS, Malvern Instruments, UK), as reported by Roy et al. (1999). Briefly, the BMP dispersion liquid (1.0 mg/mL, pH 7.0) was stirred for 1 hour and centrifuged at 2000 g for 1 min to obtain supernatant for analysis.

2.10 BMP stability analysis by multiple light scattering (MLS)

A laser diffraction scanner (Turbiscan LAB, Formulaction, Ramonville St. Agne, France) was used to determine the stability of treated BMP. The scanner was equipped with a pulse near-infrared light source (λ = 880 nm) and two synchronous detectors scanning the height of the sample. Transmission and backscatter data were collected every 40 μm. The scanning frequency was set as every 30 s in the initial 30 min, and the percentage of light backscatter or transmission was measured in the initial 30 min at 25℃. The turbiscan stability index (TSI) calculated by the Turbisoft 2.1 software was used to evaluate the stability of the BMP (Raikos et al. 2017).

2.11 Sodium dodecyl sulfate polyacrylamide gel electrophoresis (SDS-PAGE)

The composition of the treated BMP solution was determined through SDS-PAGE in which gels contained 5% and 12% polyacrylamide corresponding to application voltages of +80 V (0.5 h) and +120 V (1.0 h). Specifically, in the presence or absence of β-mercaptoethanol, 100.0 μL (1.5mg/mL) of the treated BMP solution was mixed with 50.0 μL buffer solution. Then, 10.0 μL mixture was added onto the top of the gel. After electrophoresis, the gel was stained with Coomassie brilliant blue (G-250), and was photographed after excess dye removal (Laemmli 1970).

2.12 Morphological characterization

2.12.1 Scanning electron microscopy (SEM)

The microstructure of BMP freeze-dried powder was observed under cold field emission scanning electron microscopy (S-4800, Hitachi, Tokyo, Japan). The different treated BMP powder was subjected to the same crushing treatment. The BMP powder was uniformly adhered to the conductive adhesive and observed after gold spraying.

2.12.2 Transmission electron microscopy (TEM)

The structure of BMP solution was observed at 80 kV acceleration voltage under transmission electron microscopy (Hitachi H-7650) in high contrast imaging mode. BMP was drop cast onto carbon-coated copper grid, negatively stained with 2% sodium ortho-tungstate solution for 30 s, and air dried before imaging.

2.13 Determination of hydrolysis degree

The amino acid peptide nitrogen content in enzymatic hydrolysate and raw material were determined by formaldehyde potentiometric titration (Mahmoud et al. 1992). The Bradford method was used to determine the protein concentration in raw material, and the total nitrogen content in raw material was calculated as protein concentration multiplied by conversion coefficient (6.25). The degree of hydrolysis was calculated according to the following formula.

The degree of hydrolysis = $(AN-AN_0)$ /N× 100%

where AN is the content of amino acid peptide nitrogen in enzymatic hydrolysate, AN_0 is the initial free amino acid nitrogen (not induced by enzymatic hydrolysis-naturally present in the BMP), and N is the content of total nitrogen in BMP.

2.14 Determination of antioxidant capacity

2.14.1 Scavenging effect of BMP and its enzymatic hydrolysate on DPPH

The scavenging activity of DPPH was determined by previously reported method with some modifications (Xie et al. 2008). The 2.0 mL sample solution was mixed with 2.0 mL DPPH (0.2 mM) and reacted at room temperature in the dark for 30 min. The absorbance of the mixed solution at 517 nm was measured with a spectrophotometer (L5S, Shanghai, China) and expressed as Ai. The DPPH solution was replaced with 95% ethanol, and the above operation was repeated for 3 times. The absorbance of solution (95% ethanol + BMP) was expressed as A_j. The BMP sample was replaced with ultrapure water, and the above operation was repeated for 3 times. The absorbance of solution (95% ethanol + ultrapure water) was recorded as A_c. The radical scavenging capacity was calculated by the following formula:

Inhibition (%) = $[1-(A_i-A_j)/A_c] \times 100\%$

2.14.2 Scavenging effect of BMP and its enzymatic hydrolysate on ·OH

The scavenging effect of ·OH was determined by test kits purchased from Nanjing Jiancheng Bioengineering Institute (Nanjing, China).

2.14.3 Chelation of BMP or its enzymatic hydrolysate with Fe^{2+}

The Fe^{2+} chelation was determined by the previously reported method with some modifications (Decker and Welch 1990). The 1.0 mL the sample solution, 3.7 mL ultra-pure water, 0.1 mL ferrous chloride solution (2.0 mM), and 0.2 mL of phenazine solution (5.0 mM) were mixed and reacted for 10 min. Subsequently, the absorbance of the mixture at 562 nm was measured. The ultrapure water was used as the control. The chelation ability of Fe^{2+} was calculated according to the following formula.

Chelation (%) = $[(A_{control}-A_{sample})/A_{control}] \times 100\%$

2.14.4 Reducing capacity of BMP and its enzymatic hydrolysate

The reducing capacity of BMP and its enzymatic hydrolysate was measured using the method reported by Yen and Chen (1995) with some modifications. The 2.5 mL potassium ferricyanide solution (1%), 0.5 mL BMP, and 2.5 mL phosphate-buffered saline (0.2 M, pH 6.6) were mixed and incubated at 50℃ for 20 min. Subsequently, 2.5 mL trichloroacetic acid (10%) was added, and the mixture was centrifuged at 3000 g for 10 min. The 2.5 mL supernatant, 0.5 mL ferric chloride solution (0.1%), and 2.5 mL distilled water

were mixed and reacted at room temperature for 10 min, and the absorbance of the mixture solution at 700 nm was measured with a spectrophotometer (L5S, Shanghai, China). The higher the absorbance, the stronger the sample reducibility.

2.15 Statistical Analysis

In this study, all experiments were conducted at least in triplicates, and the data were subjected to one-way ANOVA using SPSS software (SPSS 25.0, SPSS Inc., Chicago, IL). The results were expressed as means ± standard deviations (SDs), and $p < 0.05$ was considered as statistically significant.

3 Results And Discussion

3.1 Effects of high pressure treatment on BMP structure

The effects of high pressure treatment on BMP structure were examined by Fourier Transform infrared spectroscopy (FT-IR), total sulfhydryl content (SH_T), surface hydrophobicity (H_0), and intrinsic fluorescence emission spectroscopy (IFES). The FT-IR can be employed to examine BMP secondary structure change induced by high pressure treatment, and SH_T, H_0 and IFES can be used to investigate BMP tertiary structure (Shi et al. 2019).

3.1.1 FT-IR analyses

The secondary structure proportions of treated BMP obtained through FT-IR analysis, including α-helix (1650 ~ 1660 cm^{-1}), β-sheet (1600 ~ 1640 cm^{-1}), β-turn (1660 ~ 1700 cm^{-1}) and random coil (1640 ~ 1650 cm^{-1}) were shown in Supplementary Table 1 and Fig. 1A. In comparison with the control, all the treatments changed the secondary structure proportions of BMP. After UHP, HPH, and U-H treatments, α-helix and the random coil were significantly decreased ($p < 0.05$), β-sheet was significantly increased ($p < 0.05$). H-U treatment significantly decreased the α-helix content ($p < 0.05$) and significantly increased the β-sheet content ($p < 0.05$). The impact of all the treatments on the β-turn content was not significant ($p > 0.05$). The destruction of the α-helix was due to the hydrogen bond change, whereas the significant increase in β-sheet content ($p < 0.05$) and a decrease in random coil might be due to the decrease in particle size (Gaoshang et al. 2019). Similar results have been reported that UHP treatment reduced the α-helix content in myofibrillar protein from *Oratosquilla oratoria* muscle (Gaoshang et al. 2019) and increased β-sheet content in the myofibrillar protein from *Trichiurus Haumela* Surimi (Chen et al. 2020b). Shi et al. (2019) have found the β-turn proportion in the clam shell myofibrillar was decreased after HPH treatment, which was inconsistent with our results. This inconsistence might be attributed to the different pressure value and homogenization degree. In addition, our data indicated that the sequences of combined treatments (U-H and H-U) significantly affected the secondary structure in the BMP ($p < 0.05$). More random coils were observed under the H-U than under U-H. Actually, the HPH disrupted the interactions between the protein molecules by mechanical shearing (Yang et al. 2018), whereas the UHP treatment could increase the aggregation of protein molecules through hydrophobic groups (Jackson and

McGillivray 2011), which might explain the difference in secondary structure induced by different sequence of combined treatments. These results indicated that different high pressure treatments had different effects on protein structure. U-H treatment significantly destroyed the α-helix structure maintained by hydrogen bonds and facilitated the formation of β-sheet. The secondary structure of BMP was significantly changed after high pressure treatment, and they were no longer in their original natural state.

3.1.2 SH_T analyses

The total sulfhydryl content (SH_T) of BMP under different treatments were shown in Fig. 1B. In the present work, four different treatments of BMP resulted in the significant decrease in SH_T content when compared with the control ($p < 0.05$). U-H treated BMP had the lowest SH_T content (7.24 μmol/g) which was about 23% lower than that in its natural state, indicating that more disulfide bonds were formed between protein molecules. Under U-H treatment, the linear polypeptide chain of the protein further folded into a tight and stable three-dimensional structure (Xue et al. 2018). These changes were advantageous in terms of energy since the internal energy of the entire polypeptide chain with stable three-dimensional structure was reduced to the optimal minimum under the interaction of the polypeptide chain (Zhou, Lin, Liang, Benjakul, Shi, & Liu, 2014). Our SH_T result was consistent with the above-mentioned α-helix content decrease and β-sheet increase in the secondary structure under high pressure treatment. These results indicated that the freedom of the single chain was limited, and that the protein molecule became more stable (Tamashiro and Pincus 2001).

3.1.3 H_0 analyses

The hydrophobicity is a major marker of natural protein denaturation. The H_0 in four BMP treatment groups was significantly higher ($p < 0.05$) than that in the control group (Fig. 1C). The U-H-treated BMP presented the highest H_0 (924.5 ± 1.0), which was about 63% higher than that in its natural state. The denaturation of the protein under high pressure resulted in conformational changes, thus leading to the exposure of the internal hidden hydrophobic amino acid residues to protein surface, eventually increasing H_0 (He et al. 2019). Ma et al. (2021) found that the α-helix and β-sheet unfolded to different extents under the high pressure treatment, which may increase hydrophobicity. The changes of the β-sheet and β-turn under high pressure were slightly different from our experimental results, which was attributed to the transformation between the secondary structures of myofibrillar protein. The cavitation, shear stress, and high turbulence induced by HPH treatment could untie the protein or dissociate the protein aggregation, thus making the internal amino acid residues buried in the folded structure exposed to the surface of the protein and increasing H_0 (Zhang et al. 2017). The H_0 of the HPH-treated BMP (748.2 ± 1.5) was significantly higher ($p < 0.05$) than that of UHP-treated BMP (614.8 ± 1.4), suggesting shearing effect under HPH was stronger than that under UHP. When UHP and HPH were combined (U-H), H_0 shown the maximum value, which was 1.5 times as high as that in the control group due to the superposition of the two effects. This superposition effect might be due to the fact that two head S_1 and S_2 subunits of BMP were fused to form a large protein, resulting in the aggregation of BMP under the pressure and the

increase in hydrophobicity, ultimately enhancing the hydrophobic interaction of BMP (Gaoshang et al. 2019).

3.1.4 IFES analyses

Intrinsic fluorescence spectroscopy (IFES) is generally applied to detect folding state of protein (Liu et al. 2021). As shown in Fig. 1D, the fluorescence intensity of all the treatment groups was weaker than that of the control group, and the intensity of U-H treatment group was the weakest. The maximum emission peak wavelength of BMP in the control group was 338.2 nm, and the maximum emission wavelength of BMP in UHP, HPH, U-H, and H-U treatment groups were red-shifted to 339.8 nm, 340.0 nm, 340.6 nm, 340.0 nm, respectively. In general, 340nm was the maximum emission wavelength of tryptophan (Cui et al. 2014). This might be due to the fact that under high pressure, the sulfhydryl group was oxidized into disulfide bond, therefore resulting in the protein rearrangement into a special tight structure, and the hydrophilic amino acids such as tyrosine were reoriented to the interior and hydrophobic amino acid such as tryptophan were exposed to the outside, leading to the reduced the fluorescence intensity and the redshifted emission wavelength. The reduction of particle size under high pressure treatment was confirmed in the later section.

3.2 Effects of high pressure treatment on particle properties of BMP

3.2.1 Particle size analyses

As shown in Fig. 2A, the particle size distribution in the control group and U-H treatment group was unimodal, while that in the other treatment groups was bimodal, suggesting the untreated BMP and U-H treated BMP spread evenly. The particle size distribution in the control group ranged from 197 nm to 770 nm with the peak at 420.2 nm, and that in UHP, HPH, U-H, H-U treatment groups were in the range of 125 ~ 661nm, 93 ~ 568 nm, 80 ~ 661 nm, and 93 ~ 768 nm respectively. The mean particle sizes of all the treated BMPs were lower than that of the control BMP (Fig. 2B). The mean particle size in treatment groups was significantly reduced ($p < 0.05$), and that in U-H treatment group was the smallest, which was only 53% of that in the control group. This was consistent with the previous reports (Cha et al. 2018; Song et al. 2013). The differences between the control BMP and treated BMP might be ascribed to the difference in surface hydrophobicity and surface charge distribution. This might be because the high pressure treatment enhanced the interaction between protein molecules (Cha et al. 2018) and increased the surface charge (the absolute value of zeta potential increases), thus significantly decreasing protein particle size ($p < 0.05$).

3.2.2 Zeta potential analyses

Zeta potential is related to the stability of dispersion (Tan et al. 2021). High zeta potential absolute value of protein molecules indicates the smaller dispersed particles and more stable system. Zeta potential values of the control BMP and the treated BMP were shown in Fig. 2C. BMP droplets of all the samples

were negatively charged, and the absolute values of zeta potential in the treatment groups were higher than that in the control, and the maximum zeta potential absolute value (18.88 ± 0.11) was observed in the U-H treatment group ($p < 0.05$), which was 3 times of that in control group. Under high pressure treatment, spatial conformational recombination and equilibrium resulted in the increase of surface charge, thus making the protein more stable (Zhang et al. 2015). Our results agreed exceptionally well with those determined the absolute value of zeta potential of protein significantly increased after high pressure treatment (Zhao et al. 2018b).

3.2.3 MLS analyses

Turbiscan stability index (TSI) is frequently used to quantity the resistance of the protein to gravitational separation, and it is inversely proportional to the stability of the protein. As shown in Fig. 2D, all the treatments reduced the TSI value of BMP and increased its stability, when compared to the control. U-H treated BMP exhibited the lowest TSI value. High pressure treatment decreased the TSI by reducing the particle size of the BMP. This observation was consistent with the zeta potential results.

3.3 SDS-PAGE

Molecular bands of treated BMP were shown in Fig. 3. All the samples contained myosin heavy chain (200 kDa, MHC) and actin (45 kDa) (the major components of BMP) as well as several low-intensity low-molecular weight bands such as troponin-T band (35 kDa) and tropomyosin band (34 kDa). In the denaturized but not reduced condition, most band intensity of all the treated BMP was weaker than that of control BMP, and dark stains were observed on the top of numerous high-molecular-weight protein bands. In the denaturized and reduced condition, these polymers on the top of bands (dark stains) were reduced and the lost protein bands (especially MHC and actin) were recovered (Fig. 3.B), but their gray level was still lower than that of control BMP, suggesting that the high pressure treatments increased the aggregation of BMP by cross-linking of disulfide bonds, which was in line with the results of total sulfhydryl groups. Especially, band change was the most obvious in the two combined treatments (U-H and H-U). In addition, some high-molecular-weight polymers were observed in the control group and UHP group, which might result from the interactions between functional group, such as tyrosine-tyrosine interaction, carbonyl-amino interaction (Estevez 2011). Figure 3B showed that the intensity of low-molecular-weight bands (troponin-T and tropomyosin) of treated BMP was increased in comparison with that of the control BMP, indicating that large-molecular-weight proteins in BMP were degraded into small sub-fragments after high pressure treatment (Grossi et al. 2016). Martínez et al. (2017) found that UHP could promote dissociation of MHC, and that the low-molecular-weight bands presented molecular weight between 45 kDa and 100 kDa in the crab meat. Chen et al. (2020b) presented that high pressure affected the composition of myofibrillar protein and partially degraded the actin and myosin heavy chain. Su et al. (2021) reported that the impact of HPH on myofibrillar proteins included both aggregation and depolymerization, and when myofibrillar proteins was treated with HPH, the MHC gradually disappeared and new band with the molecular weight of about 245 kDa and 75 kDa formed. In our study, the results of mean particle size also confirmed the depolymerization of HHP treated BMP. Compared to U-H treated

BMP, H-U treated BMP exhibited a low-molecular-weight bands (actin, troponin-T, and tropomyosin) with decreased intensity and the high-molecular-weight bands (MHC) with increased intensity, which was attributed to the aggregation of high molecular weight proteins after H-U treatment.

3.4 Micro-morphology characterization

3.4.1 SEM

SEM results of control and treated BMP powder were depicted in Fig. 4. At low magnification (500 folds), the control and UPH treated BMP presented a large chunk-like structure, while the HPH, U-H and H-U treated BMP displayed loose fragment structure. The structure of UPH treated BMP was more compact than that of the control BMP. At high magnification (2000 folds), the control and four treated BMP exhibited four types of structure including rod-like structure in the control, chunk-like structure in the UHP treated BMP, lamellar structures in the BMP after HPH and U-H treatment, fragment-like structure in H-U treated BMP. As shown in Fig. 4a, the orderly rod-like structure was observed in control BMP. Cross-linking between proteins were found in the UHP and H-U treated BMP. These microstructure changes might be due to cavitation and shear effects induced by HPH, which disrupted the electrostatic and hydrophobic interactions between BMP molecules, thus reducing the particle size and stabilizing the protein structure (Zhao et al. 2018a). Protein molecular crosslinking was destroyed under the treatment of UHP, and the protein underwent micro-variation (Liu et al. 2011). The irregular pores were formed on the surface of the lamellar structure, which might be ascribed to the rapid evaporation of moisture (Liu et al. 2021).

3.4.2 TEM

As shown in Fig. 5A and 5a, the control exhibited an obvious relatively homogeneous net-like structure. Regular structures of myofibrillar protein have also been reported in other studies (Li et al. 2019; Chen et al. 2016; Ito et al. 2003). As shown in Fig. 5, under UHP, HPH, and U-H treatments, BMP exhibited small particles with diameters of approximately 200 nm, which might be monodispersed or oligomer. Our results were similar to the previous report that the length of BMP ranged from approximately 100–400 nm after HPH treatment (Li et al. 2019). Figure 5B and 5b showed numerous agglomerates, indicating that the original filamentous structures of the BMP might be compressed to agglomerates by UHP. In addition, BMP particles were evenly dispersed under HPH and U-H treatments (Fig. 5c and 5d), while the H-U treated BMP displayed flocculent distribution. The particles in the U-H treated BMP were larger than those in HHP treated BMP. The obtained BMP diameters in the TEM images failed to completely correspond to the results of mean particle size, which might be due to the limitation of sample preparation and TEM views.

3.5 Effects of high pressure treatments on hydrolysis degree and antioxidant activity

As shown in the Table 1, BMP under different treatments exhibited significantly different hydrolysis degrees ($P < 0.05$). The hydrolysis degree of U-H treated BMP was the highest, followed by UHP, HPH, and H-U treated BMP. The results showed that non-hydrolyzed BMP exhibited low antioxidant activity (Supplementary Table 2), but enzymatic hydrolysis significantly improved the antioxidant activity of BMP ($P < 0.05$). Among all the groups, the enzymic hydrolysates in U-H treatment group exhibited the highest antioxidant activity. Specifically, under U-H treatment, the scavenging effect of DPPH increased from 54.5–65.9%, the scavenging effect of ·OH increased from 54.7 U/mL to 59.3 U/mL, the chelation of Fe^{2+} increased from 11.9–27.1%, and the reducing capacity increased from 0.27A to 0.33A. Consistently, the promotion effects on antioxidant activity have been reported in the enzymatic hydrolysates of UHP treated lentil proteins (Garcia-Mora et al. 2015) and those of HPH treated sardine proteins (Rivero-Pino et al. 2020). Previous study has indicated that before high pressure treatment, the compact tertiary structure of protein molecules is responsible for their unease to combine the protease (Guan et al. 2018), resulting in a low hydrolysis degree and antioxidant activity. As shown in the Fig. 6, under UHP treatment, high pressure destroyed the biological tissue and caused protein denaturation, but insufficient protein particle size reduction resulted in decrease in the protease-mediated degradation of proteins (Li et al. 2021a). Under HPH treatment, although strong shear force sufficiently reduced particle sizes of protein molecules and enhanced intermolecular electrostatic repulsion, but the internal sulfhydryl group was not completely exposed, thus resulting in inadequate protein degradation (Chen et al. 2020a). Based on these findings, we hypothesized under the H-U combined treatment, the BMP first obtained small and dispersed particles from HPH treatment, then the subsequent UHP treatment increased the BMP particle size and hid hydrophobic groups in BMP aggregates, thus making it difficult for protease to bind with BMP. However, enzymatic hydrolysates in U-H pretreated BMP showed the highest hydrolysis degree and antioxidant activity, which might be ascribed to the following favorable structural changes. Firstly, U-H treatment could destroy the hydrogen bonds in BMP to the greatest extent; Secondly, U-H treatment could expose sulfhydryl and hydrophobic groups to the maximum extent; Finally, U-H treatment could degrade high-molecular-weight BMP, decrease the particle size of protein, increase zeta potential absolute value, improve the BMP stability, thus maximizing the possibility of enzyme contact with the sample. These changes made it easy for pepsin to enter the BMP molecule under high pressure, thus increasing hydrolysis degree of BMP sample and the antioxidant capacity of enzymatic hydrolysates.

Table 1
Hydrolysis degree and antioxidant activity under different high pressure treatments

Treatment	Degree of hydrolysis (%)	Antioxidant activity of enzyme hydrolysates			
		Scavenging effect of DPPH (%)	Scavenging effect of ·OH (U/ml)	Chelation of Fe^{2+} (%)	Reducing capacity(A)
Control	43.0 ± 0.5^{a}	54.5 ± 1.1^{a}	54.7 ± 0.2^{a}	11.9 ± 0.9^{a}	0.27 ± 0.005^{a}
UHP	50.8 ± 0.9^{c}	64.0 ± 0.4^{c}	55.4 ± 0.6^{a}	20.7 ± 1.1^{b}	0.29 ± 0.003^{b}
HPH	46.6 ± 0.4^{b}	59.2 ± 1.2^{b}	55.1 ± 0.3^{a}	22.3 ± 0.5^{b}	0.3 ± 0.009^{c}
U-H	54.4 ± 1.6^{d}	65.9 ± 1.1^{d}	59.3 ± 0.5^{c}	27.1 ± 1.9^{c}	0.33 ± 0.003^{e}
H-U	43.0 ± 0.7^{a}	63.2 ± 0.3^{c}	56.6 ± 0.3^{b}	21.7 ± 1.4^{b}	0.32 ± 0.005^{d}
Note: Different letters represent significant differences at $P < 0.05$.					

4 Conclusions

In this study, four different treatments (UHP, HPH, U-H, and H-U) were applied to the BMP. We found that the treatment methods had a great influence on the hydrogen bonds, sulfhydryl, hydrophobic groups, and molecular weight of BMP, thus making the enzyme easily enter the BMP molecule under pressure. The destruction of the hydrogen bond of BMP resulted in a decrease in the α-helix content and an increase in β-sheet. The exposure of sulfhydryl resulted in the formation of disulfide bonds, which enabled BMP to form a compact stable three-dimensional structure. This was verified by the improvement in the stability of BMP solution, the reduction in the fluorescence intensity, and the reduction in particle size of BMP. The exposure of the hydrophobic groups increased the surface hydrophobicity. SDS-PAGE results indicated that the molecular weight of BMP was decreased after high pressure treatment. At microstructure level, SEM and TEM results confirmed the above structural changes. All the high pressure treatments promoted hydrolysis degree and antioxidant activity of the enzymatic hydrolysates, and the U-H treatment was found to be the most effective. These results can provide evidence for increasing the antioxidant activity of the hydrolysate under different high pressure treatments. Future studies are suggested to further isolate, purify, and identify the structure of the peptide so as to identify the peptide fragments with the main antioxidant activity from the enzymatic hydrolysate.

Declarations

Author's contribution

Mengting Chen performed the experiment, performed the data analyses and wrote the manuscript,

Lan Wang and Bijun Xie contributed to the conception of the study,

Wenjin Wu and Zhida Sun contributed significantly to analysis and manuscript preparation,

Changliang Zheng, Aimin Ma, Liu Shi, Anzi Ding, Guangquan Xiong, Yu Qiao and Xin Li helped perform the analysis with constructive discussions.

Funding Declaration

The research was funded by the National Key R&D Program of China (2019YFD0901805).

Conflict of Interest Statement

The authors declare that they do not have any known competing financial interests or personal relationships.

Data Availability Statement

The data that support the findings of this study are available from the corresponding author upon reasonable request.

References

1. Cha Y, Wu F, Zou H, Shi X, Zhao Y, Bao J, Du M & Yu C (2018) High-Pressure Homogenization Pre-Treatment Improved Functional Properties of Oyster Protein Isolate Hydrolysates. Molecules. 23(12).
2. Chen X, Liang L & Xu X (2020a) Advances in converting of meat protein into functional ingredient via engineering modification of high pressure homogenization. Trends in Food Science & Technology. 106, 12–29.
3. Chen X, Xu X & Zhou G (2016) Potential of high pressure homogenization to solubilize chicken breast myofibrillar proteins in water. Innovative Food Science & Emerging Technologies. 33, 170–179.
4. Chen Y, Xu A, Yang R, Jia R, Zhang J, Xu D & Yang W (2020b) Myofibrillar Protein Structure and Gel Properties of Trichiurus Haumela Surimi Subjected to High Pressure or High Pressure Synergistic Heat. Food and Bioprocess Technology. 13(4), 589–598.
5. Cui Z, Kong X, Chen Y, Zhang C & Hua Y (2014) Effects of rutin incorporation on the physical and oxidative stability of soy protein-stabilized emulsions. Food Hydrocolloids. 41, 1–9.
6. Dai W, Gu S, Xu M, Wang W, Yao H, Zhou X & Ding Y (2021) The effect of tea polyphenols on biogenic amines and free amino acids in bighead carp (Aristichthys nobilis) fillets during frozen storage. LWT - Food Science and Technology. 150.
7. Decker EA & Welch B (1990) Role of ferritin as a lipid oxidation catalyst in muscle food. Journal of Agricultural and Food Chemistry. 38(3), 674–677.

8. Estevez M (2011) Protein carbonyls in meat systems: a review. Meat Science. 89(3), 259–279.
9. Gaoshang L, Yanting C, Shifen X, Mingchun L, Jinjie Z, Qiaoming L, Ru J & Yang W (2019) Effects of ultra-high pressure on the biochemical properties and secondary structure of myofibrillar protein from *Oratosquilla oratoria* muscle. Journal of Food Process Engineering. 42(6).
10. Garcia-Mora P, Penas E, Frias J, Gomez R & Martinez-Villaluenga C (2015) High-pressure improves enzymatic proteolysis and the release of peptides with angiotensin I converting enzyme inhibitory and antioxidant activities from lentil proteins. Food Chemistry. 171, 224–232.
11. Grossi A, Olsen K, Bolumar T, Rinnan A, Ogendal LH & Orlien V (2016) The effect of high pressure on the functional properties of pork myofibrillar proteins. Food Chemistry. 196, 1005–1015.
12. Guan H, Diao X, Jiang F, Han J & Kong B (2018) The enzymatic hydrolysis of soy protein isolate by Corolase PP under high hydrostatic pressure and its effect on bioactivity and characteristics of hydrolysates. Food Chemistry. 245, 89–96.
13. Guo G, Dong S, Zhao W & Chen W (2008) Fatty Acid Composition of Plankton and Bighead Carp (Aristichthys nobilis) in Freshwater Ponds. CLEAN – Soil, Air, Water. 36(2), 209–215.
14. Haskard CA & Li-Chan ECY (1998) Hydrophobicity of bovine serum albumin and ovalbumin determined using uncharged (PRODAN) and anionic (ANS(-)) fluorescent probes. Journal of Agricultural and Food Chemistry. 46(7), 2671–2677.
15. He D, Wang X, Ai M, Kong Y, Fu L, Zheng B, Song H & Huang Q (2019) Molecular mechanism of high-pressure processing for improving the quality of low-salt Eucheuma spinosum chicken breast batters. Poult Science. 98(6), 2670–2678.
16. Ito Y, Tatsumi R, Wakamatsu J-i, Nishimura T & Hattori A (2003) The solubilization of myofibrillar proteins of vertebrate skeletal muscle in water. Animal Science Journal. 74(5), 417–425.
17. Jackson AJ & McGillivray DJ (2011) Protein aggregate structure under high pressure. Chem Commun (Camb). 47(1), 487–489.
18. Laemmli UK (1970) Cleavage of structural proteins during the assembly of the head of bacteriophage T4. Nature. 227(5259), 680.
19. Li S, Wang Y, Xue Z, Jia Y, Li R, He C & Chen H (2021a) The structure-mechanism relationship and mode of actions of antimicrobial peptides: A review. Trends in Food Science & Technology. 109, 103–115.
20. Li X, Li S, Shi G, Xiong G, Shi L, Kang J, Su J, Ding A, Li X, Qiao Y, Liao L, Wang L & Wu W (2021b) Quantitative proteomics insights into gel properties changes of myofibrillar protein from Procambarus clarkii under cold stress. Food Chemistry.
21. Li Y, Chen X, Xue S, Li M, Xu X, Han M & Zhou G (2019) Effect of the disruption chamber geometry on the physicochemical and structural properties of water-soluble myofibrillar proteins prepared by high pressure homogenization (HPH). LWT - Food Science and Technology. 105, 215–223.
22. Liu CM, Zhong JZ, Liu W, Tu ZC, Wan J, Cai XF & Song XY (2011) Relationship between functional properties and aggregation changes of whey protein induced by high pressure microfluidization. Journal of food science. 76(4), E341-347.

23. Liu G, Xiong YL & Butterfield DA (2000) Chemical, physical, and gel-forming properties of oxidized myofibrils and whey- and soy-protein isolates. Journal of food science. 65(5), 811–818.
24. Liu Z, Guo Z, Wu D, Fei X, Ei-Seedi HR & Wang C (2021) High-pressure homogenization influences the functional properties of protein from oyster (Crassostrea gigas). LWT - Food Science and Technology. 151.
25. Ma R, Liu H, Li Y, Atem BJA, Ling X, He N, Che L, Wu X, Wang Y & Lu Y (2021) Effects of High Hydrostatic Pressure Treatment: Characterization of Eel (Anguilla japonica) Surimi, Structure, and Angiotensin-Converting Enzyme Inhibitory Activity of Myofibrillar Protein. Food and Bioprocess Technology. 14(9), 1631–1639.
26. Mahmoud MI, Malone WT & Cordle CT (1992) Enzymatic hydrolysis of Casein. Effect of degree of hydrolysis on antigenicity and physical properties. Journal of food science. 57(5), 1223–1229.
27. Martínez MA, Velazquez G, Cando D, Núñez-Flores R, Borderías AJ & Moreno HM (2017) Effects of high pressure processing on protein fractions of blue crab (Callinectes sapidus) meat. Innovative Food Science & Emerging Technologies. 41, 323–329.
28. Masomeh Ghassem KA, Abdul Salam Babji, Mamot Said, Saadiah Ibrahim (2011) Purification and identification of ACE inhibitory peptides from Haruan (Channastriatus) myofibrillar protein hydrolysate using HPLC–ESI-TOF MS/MS. Food Chemistry. 129, 1770–1777.
29. Raikos V, Duthie G & Ranawana V (2017) Comparing the efficiency of different food-grade emulsifiers to form and stabilise orange oil-in-water beverage emulsions: influence of emulsifier concentration and storage time. International Journal of Food Science & Technology. 52(2), 348–358.
30. Rivero-Pino F, Espejo-Carpio FJ & Guadix EM (2020) Bioactive fish hydrolysates resistance to food processing. LWT - Food Science and Technology. 117.
31. Roy K, Mao HQ, Huang SK & Leong KW (1999) Oral gene delivery with chitosan-DNA nanoparticles generates immunologic protection in a murine model of peanut allergy. Nature Medicine. 5(4), 4.
32. Ryan JT, Ross RP, Bolton D, Fitzgerald GF & Stanton C (2011) Bioactive peptides from muscle sources: meat and fish. Nutrients. 3(9), 765–791.
33. Saricaoglu FT, Gul O, Besir A & Atalar I (2018) Effect of high pressure homogenization (HPH) on functional and rheological properties of hazelnut meal proteins obtained from hazelnut oil industry by-products. Journal of Food Engineering. 233, 98–108.
34. Sharifian A, Soltanizadeh N & Abbaszadeh R (2019) Effects of dielectric barrier discharge plasma on the physicochemical and functional properties of myofibrillar proteins. Innovative Food Science & Emerging Technologies. 54, 1–8.
35. Shi X, Zou H, Sun S, Lu Z, Zhang T, Gao J & Yu C (2019) Application of high-pressure homogenization for improving the physicochemical, functional and rheological properties of myofibrillar protein. International Journal of Biological Macromolecules. 138, 425–432.
36. Song X, Zhou C, Fu F, Chen Z & Wu Q (2013) Effect of high-pressure homogenization on particle size and film properties of soy protein isolate. Industrial Crops and Products. 43, 538–544.

37. Su C, He Z, Wang Z, Zhang D & Li H (2021) Aggregation and deaggregation: The effect of high-pressure homogenization cycles on myofibrillar proteins aqueous solution. International Journal of Biological Macromolecules. 189, 567–576.
38. Sunil, Chauhan N, Singh J, Chandra S, Chaudhary V & Kumar V (2018) “Non-thermal techniques: Application in food industries” A review. Journal of Pharmacognosy and Phytochemistry. 7(5), 1507–1518.
39. Tamashiro MN & Pincus P (2001) Helix-coil transition in homopolypeptides under stretching. Phys Rev E Stat Nonlin Soft Matter Phys. 63(2 Pt 1), 021909.
40. Tan M, Xu J, Gao H, Yu Z, Liang J, Mu D, Li X, Zhong X, Luo S, Zhao Y, Jiang S & Zheng Z (2021) Effects of combined high hydrostatic pressure and pH-shifting pretreatment on the structure and emulsifying properties of soy protein isolates. Journal of Food Engineering. 306.
41. Tsumura K, Saito T, Tsuge K, Ashida H, Kugimiya W & Inouye K (2005) Functional properties of soy protein hydrolysates obtained by selective proteolysis. LWT - Food Science and Technology. 38(3), 255–261.
42. Ulug SK, Jahandideh F & Wu J (2021) Novel technologies for the production of bioactive peptides. Trends in Food Science & Technology. 108, 27–39.
43. Wen C, Zhang J, Zhang H, Duan Y & Ma H (2020) Plant protein-derived antioxidant peptides: Isolation, identification, mechanism of action and application in food systems: A review. Trends in Food Science & Technology. 105, 308–322.
44. Xie Z, Huang J, Xu X & Jin Z (2008) Antioxidant activity of peptides isolated from alfalfa leaf protein hydrolysate. Food Chemistry. 111(2), 370–376.
45. Xing L, Liu R, Cao S, Zhang W & Guanghong Z (2019) Meat protein based bioactive peptides and their potential functional activity: a review. International Journal of Food Science & Technology. 54(6), 1956–1966.
46. Xue S, Xu X, Shan H, Wang H, Yang J & Zhou G (2018) Effects of high-intensity ultrasound, high-pressure processing, and high-pressure homogenization on the physicochemical and functional properties of myofibrillar proteins. Innovative Food Science & Emerging Technologies. 45, 354–360.
47. Yang J, Liu G, Zeng H & Chen L (2018) Effects of high pressure homogenization on faba bean protein aggregation in relation to solubility and interfacial properties. Food Hydrocolloids. 83, 275–286.
48. Yen GC & Chen HY (1995) Antioxidant activity of various tea extracts in relation to their antimutagenicity. Journal of Agricultural and Food Chemistry. 43(1), 27–32.
49. Zhang Z, Yang Y, Tang X, Chen Y & You Y (2015) Chemical forces and water holding capacity study of heat-induced myofibrillar protein gel as affected by high pressure. Food Chemistry. 188, 111–118.
50. Zhang Z, Yang Y, Zhou P, Zhang X & Wang J (2017) Effects of high pressure modification on conformation and gelation properties of myofibrillar protein. Food Chemistry. 217, 678–686.
51. Zhao F, Zhang D, Li X & Dong H (2018a) High-Pressure Homogenization Pretreatment before Enzymolysis of Soy Protein Isolate: the Effect of Pressure Level on Aggregation and Structural

Conformations of the Protein. Molecules. 23(7).

52. Zhao Z-K, Mu T-H, Zhang M & Richel A (2018b) Chemical Forces, Structure, and Gelation Properties of Sweet Potato Protein as Affected by pH and High Hydrostatic Pressure. Food and Bioprocess Technology. 11(9), 1719–1732.
53. Zou H, Zhao N, Shi X, Sun S & Yu C (2020) Modifying the Physicochemical and Functional Properties of Water-soluble Protein from Mussels by High-pressure Homogenization Treatment. International Journal of Food Engineering. 16(3).

Figures

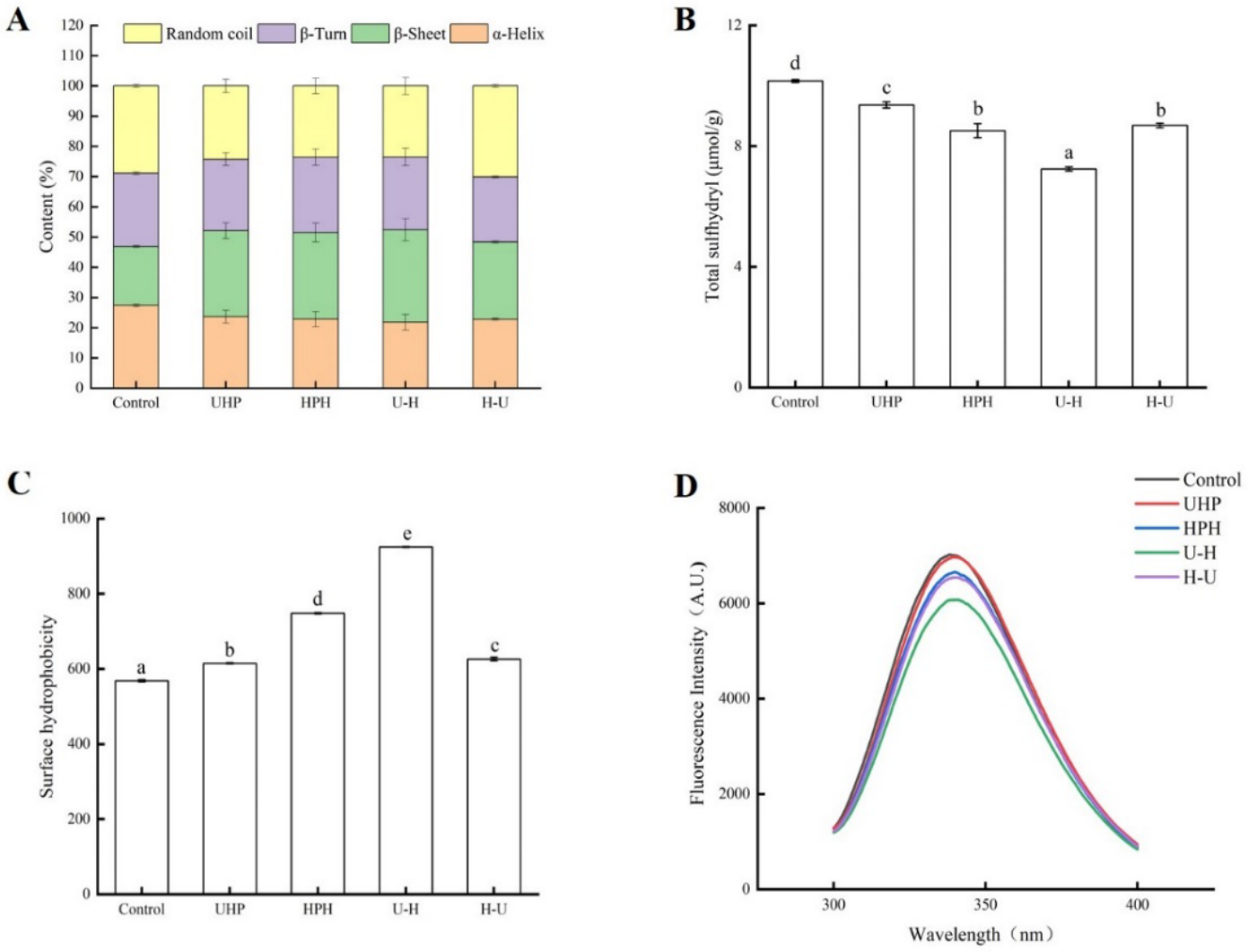

Figure 1

Structure changes of treated or untreated BMP. (A) Secondary structure. (B) Total sulfhydryl. (C) Surface hydrophobicity. (D) Intrinsic emission fluorescence spectroscopy. Different lower-case letters represent significant differences at the level of $P < 0.05$.

Figure 2

Particle size properties under different high pressure treatments. (A) Particle size distribution. (B) Mean particle size. (C) Zeta potential. (D) Turbiscan stability index (TSI). Different lower-case letters represent significant differences at the level of $P < 0.05$.

Figure 3

Representative SDS-PAGE patterns. Samples were prepared in the (A) absence or (B) presence of β-mercaptoethanol. MHC, myosin heavy chain.

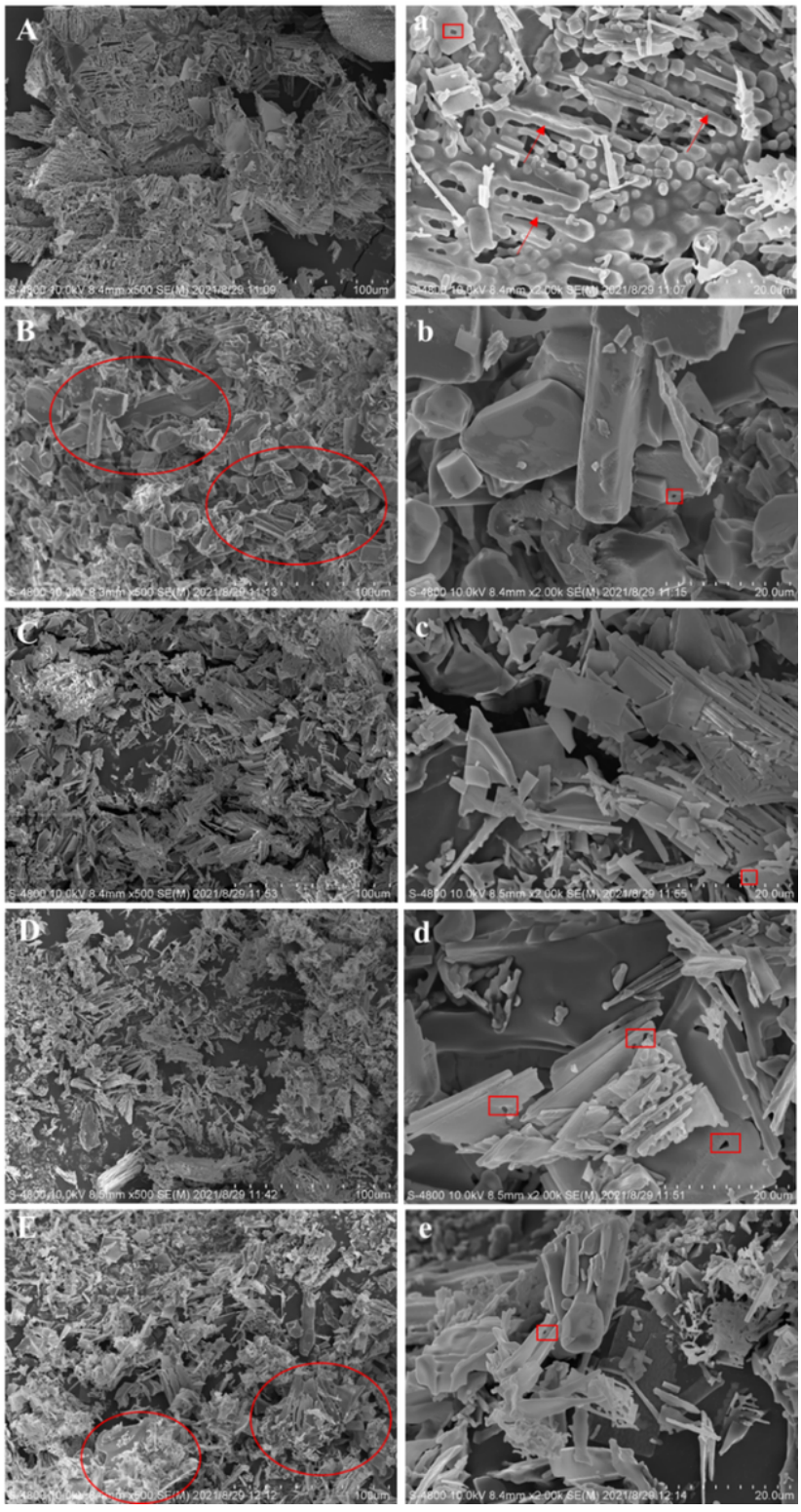

Figure 4

Scanning electron microscope images of samples under different treatments The letters represent control (A, a), UHP (B, b), HPH (C, c), U-H (D, d), H-U (E, e) respectively. Uppercase letters indicate 500-fold magnification, and lowercase letters denote 2000-fold magnification. Arrow indicates BMP rod-like structure. Circle represents the adhesions of proteins. Frame shape denotes irregular pores.

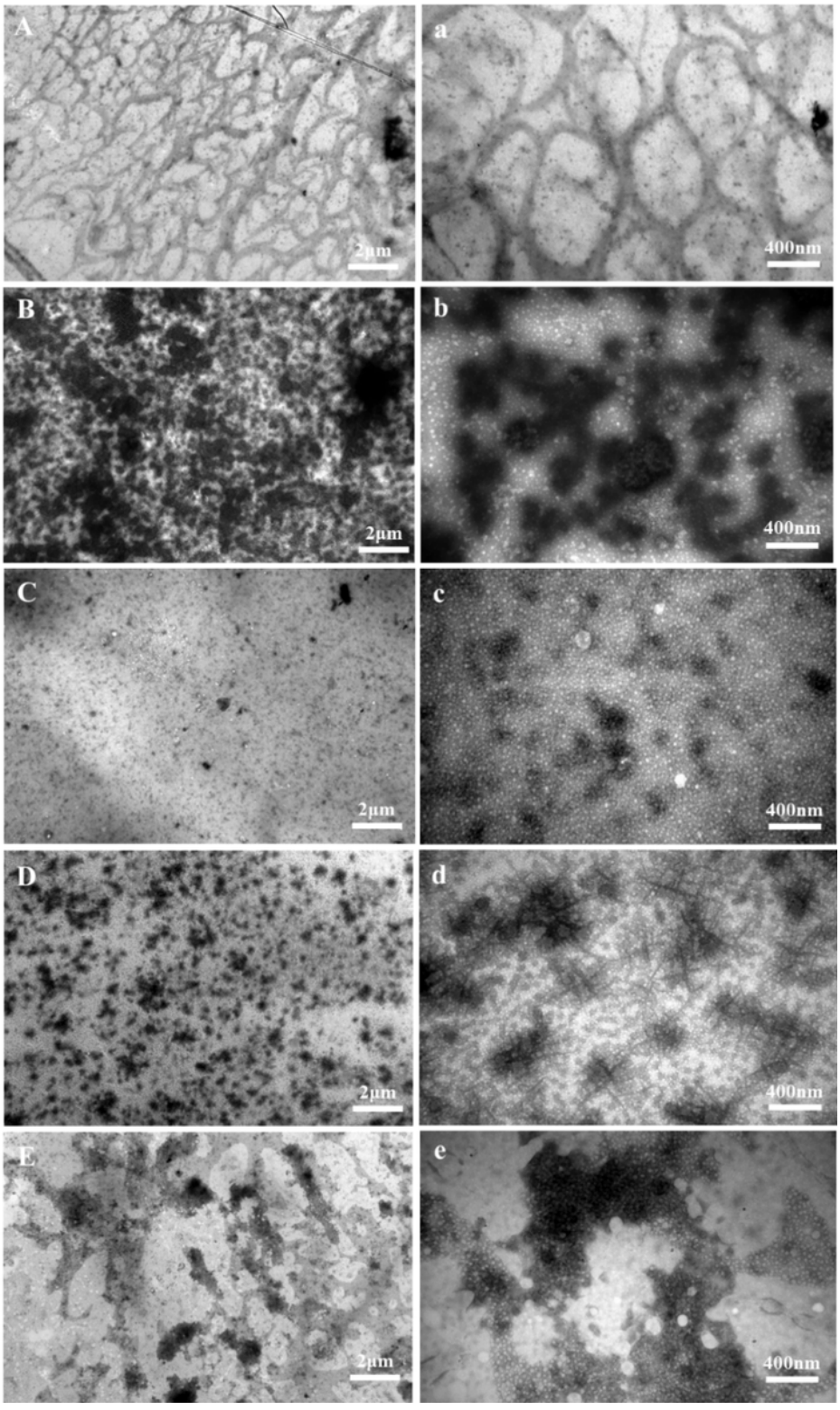

Figure 5

Transmission electron microscopy (Ma et al.) images of samples under different treatments. (A, a) Control. (B, b) UHP. (C, c) HPH. (D, d) U-H. (E, e) H-U. Uppercase letters indicate 10000-fold magnification, and lowercase letters denote 60000-fold magnification.

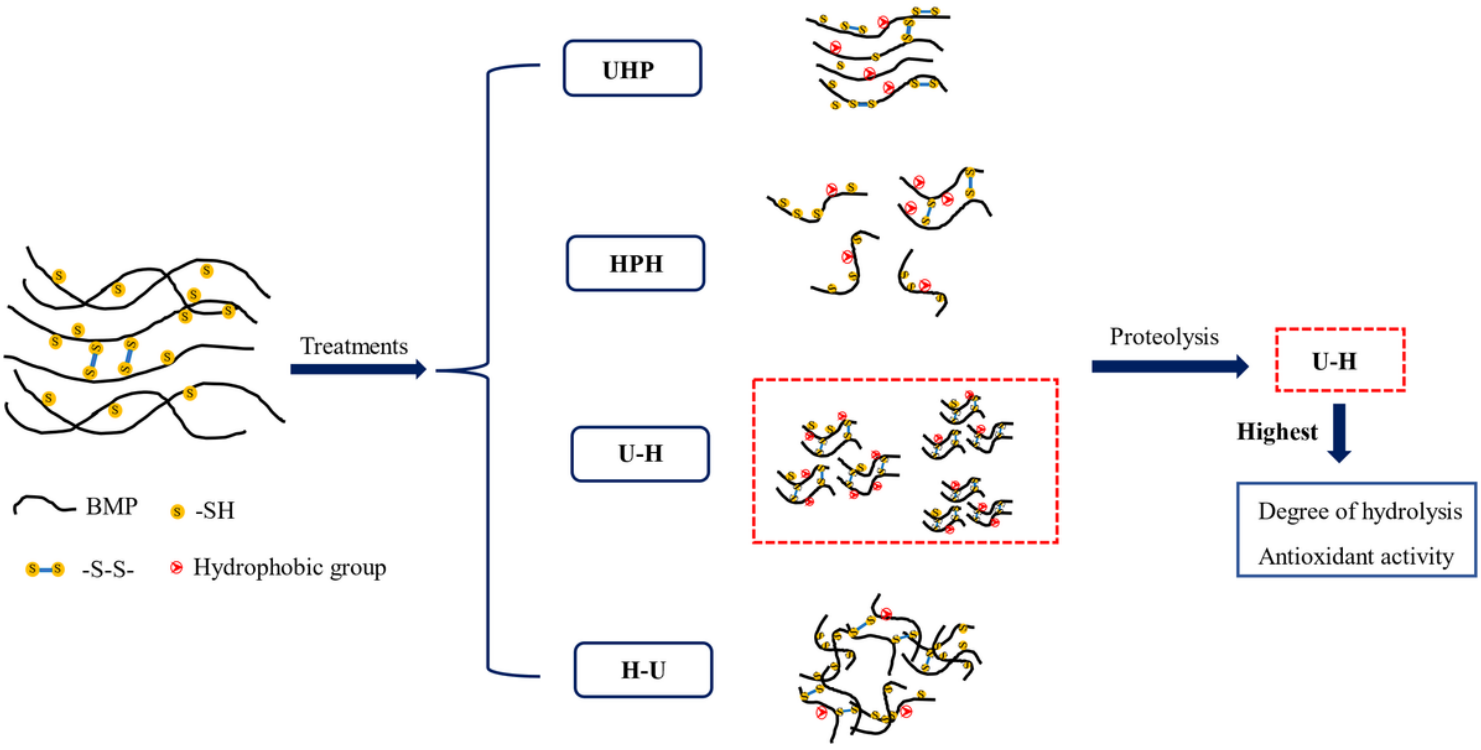

Figure 6

Schematic diagram of BMP structure changes under different high pressure treatments

Supplementary Files

This is a list of supplementary files associated with this preprint. Click to download.

- SupplementaryTables.docx